








Enhanced d - p hybridization intertwined with anomalous ground state formation in the van der Waals itinerant magnet Fe_5GeTe_2

K. Yamagami ^{1,*}, Y. Fujisawa ¹, M. Pardo-Almanza ¹, B. R. M. Smith ¹, K. Sumida ², Y. Takeda ², and Y. Okada ¹

¹Okinawa Institute of Science and Technology (OIST) Graduate University, Tancha, Onna-son, Kunigami-gun Okinawa, 904-0495, Japan

²Materials Sciences Research Center, Japan Atomic Energy Agency (JAEA), Sayo-cho, Sayo-gun, Hyogo 679-5148, Japan



(Received 15 March 2022; revised 11 June 2022; accepted 17 June 2022; published 25 July 2022)

Fe_5GeTe_2 is a van der Waals (vdW)-coupled unconventional ferromagnetic metal with a high Curie temperature (T_C) exceeding 300 K. The formation of an anomalous ground state significantly below T_C has received considerable attention, resulting in increased interest in understanding the spin-polarized electronic state evolution near the Fermi energy (E_F) as a function of temperature. Despite recent extensive studies, a microscopic understanding of the spin-polarized electronic structure around E_F has not yet been established owing to the intrinsic complexity of both the crystal and band structures. In this study, we investigate the temperature dependence of element-specific soft x-ray magnetic circular dichroism (XMCD). A systematic temperature evolution in the XMCD signal from both magnetic Fe and its ligand Te is clearly observed. More importantly, the enhancement in the hybridization between the Fe $3d$ and Te $5p$ states at low temperature in the zero-magnetic field limit is revealed. We discuss the implications of our observation in line with possible emergence of an exotic magnetic ground state in Fe_5GeTe_2 .

DOI: [10.1103/PhysRevB.106.045137](https://doi.org/10.1103/PhysRevB.106.045137)

I. INTRODUCTION

Materials hosting the coexistence of electronic conduction and magnetic order have been a crucial platform for identifying and investigating exotic correlated phases [1–3]. Magnetism typically originates from partially filled and relatively localized d or f electron orbitals in transition metals or rare-earth elements. By controlling their hybridization with delocalized ligand s and/or p orbitals, the physics of correlated systems can be enriched [1,2,4–8]. One of the most exotic cases is cuprates, in which the control of hybridization between Cu $3d$ and oxygen $2p$ orbitals (d - p hybridization) is crucial for controlling the competition of multiple exotic phases [9,10]. Heavy fermion (HF) systems are another good example, in which hybridization between f electron orbitals from rare-earth elements and conduction electrons (often known as c - f hybridization) is crucial for tuning the system from a magnetically ordered state to an HF state [4–8]. The recent surge in interest in identifying exotic metallic states in van der Waals (vdW)-coupled magnetic systems [11–13] necessitates an understanding and control of the hybridization between magnetic localized and nonmagnetic delocalized electronic orbitals. However, such an understanding has not been well developed, partly due to the limited number of vdW materials hosting both the electronic conductivity and magnetic order.

Recently, the Fe_nGeTe_2 ($n = 3, 4, 5$) family has received considerable interest as a promising vdW material series for

hosting the coexistence of electronic conduction and magnetic ordering [14–27]. Within this group, various topologically nontrivial states and consequent exotic transport phenomena have been observed [28]. Fe_5GeTe_2 is of particular interest owing to its high Curie temperature (T_C) [see Fig. 1(a) for the structure]. The Fe_5GeTe_2 system has been recognized to host unconventional ferromagnetism [19,20], whose microscopic spin structure can be better understood as antiferromagnetism or ferrimagnetism [29]. In addition to the topologically nontrivial magnetic state [28], the formation of various intriguing ground states has been argued for Fe_5GeTe_2 and its related compounds. For example, charge density wave (CDW) formation [25,30] and HF formation [22,31] have been discussed for this system below ~ 150 K (which is significantly below T_C). These observations highlight the importance of the hybridization degree, as in HF systems [4–8]. However, understanding hybridization has been not well understood in Fe_5GeTe_2 , even though the intrinsically cleavable nature of this crystal should facilitate surface-sensitive high-resolution single-particle spectroscopy. In particular, the challenge is attributed to the intrinsic chemical complexity of Fe_5GeTe_2 [32–35]. It is known that 50% of Fe(1) sites are vacant even for the stoichiometric composition Fe_5GeTe_2 [see the circle marked by the partially occupied region denoted in color for the Fe(1) site in Fig. 1(a)], in addition to the fact that the material tends to be invariably off-stoichiometrically deficient in Fe (e.g., $\text{Fe}_{5-x}\text{GeTe}_2$) [19,20,23]. The structural freedom of the Fe atoms occupying the Fe(1) sites inherently complicates the band structure, which prevents determining the degree of hybridization using angle-resolved photoemission spectroscopy [30]. Hence, an alternative probe is required to determine the hybridization strength of the entire system, without considering the complex band structure.

*Present address: Japan Synchrotron Radiation Research Institute (JASRI), 1-1-1, Sayo-cho, Sayo-gun, Hyogo 679-5198, Japan; kohei.yamagami@spring8.or.jp

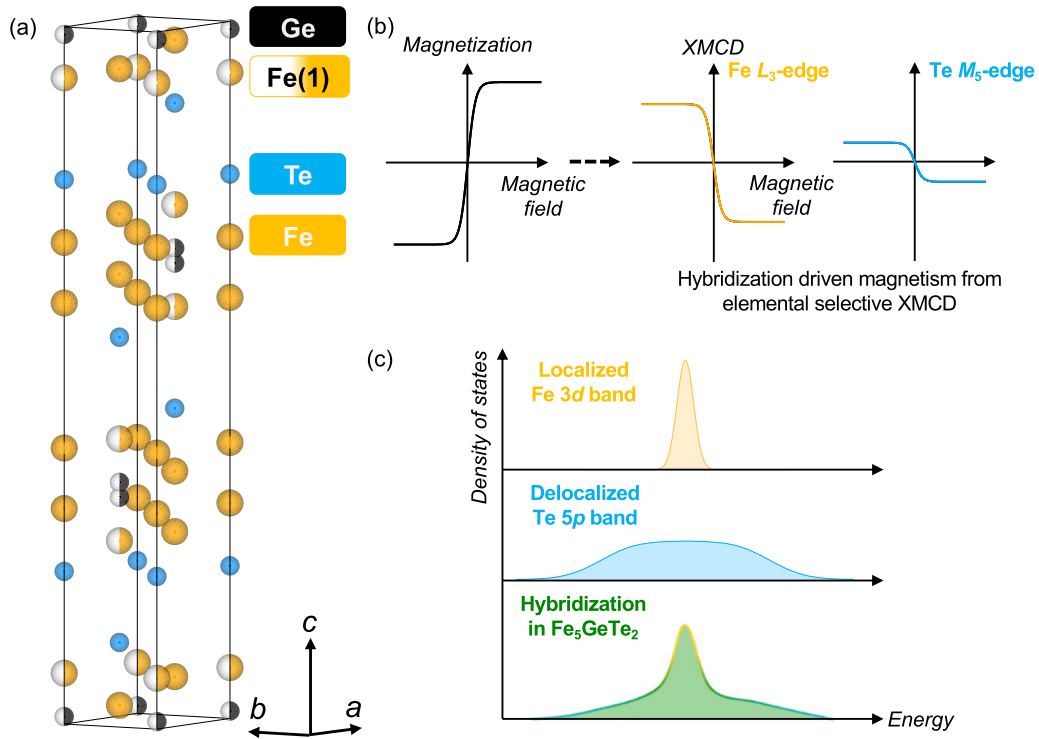


FIG. 1. (a) Crystal structure of Fe_5GeTe_2 . Solid black lines correspond to the unit cell. In Fe_5GeTe_2 , 50% split occupation for Fe(1) and Ge sites is known [19,20,23]. (b) Schematic illustration showing element-selective magnetization curves for Fe 3d (yellow) and Te 5p (light blue) states measured via XMCD for Fe_5GeTe_2 , which constitute the bulk magnetization curve (black). XMCD signal from Te is associated with a hybridization-induced origin, as per the literature [34]. Sign of XMCD signal is opposite compared with bulk magnetization curves owing to definition of obtained XMCD spectra in circularly polarized x-ray absorption measurement under external magnetic field (see main text for details). (c) Schematic illustration of localized Fe 3d (yellow) and delocalized Te 5p (light blue) states, together with hybridized states between those orbitals (green), as obtained from the literature [34]. When the hybridization was weak, the bandwidths of Fe 3d and Te 5p were narrow and wide, respectively. By contrast, when the hybridization became stronger, the band properties of both were included, and Fe 3d and Te 5p became broader and narrower, respectively. Herein, we refer to this relationship as the countereffect.

X-ray magnetic circular dichroism (XMCD) measurements have recently been demonstrated as effective for understanding the complexity of Fe_5GeTe_2 [34]. XMCD measurements provide information regarding element-specific (orbital-selective) spin-polarized electronic density of states $N(\uparrow_{\text{major}}) - N(\downarrow_{\text{minor}})$, including those in the vicinity of E_F , as a function of the external magnetic field. Therefore, element-specific magnetization curves were obtained. It was demonstrated that the XMCD-based magnetization curve shapes for Fe 3d and Te 5p were consistent with the bulk magnetometry curves [Fig. 1(b)], while considering the fact that the orbital-dependent excitation process in the XMCD measurement merely reverses the sign of the XMCD signal [34]. This observation was interpreted as a consequence of hybridization-induced magnetism in the Te 5p states, since the localized Fe 3d orbital and delocalized ligand Te 5p orbital are expected to coexist near E_F [Fig. 1(c)] (see also Ref. [34]). Therefore, the degree of d - p hybridization near E_F can be probed sensitively via element-specific XMCD measurements in complex systems such as Fe_5GeTe_2 . The previous XMCD study was performed only at 20 K, and a temperature-dependent study is yet to be conducted. Herein, we present a study pertaining to the temperature and magnetic field evolution of element-specific XMCD in Fe_5GeTe_2 ,

where enhanced p - d hybridization significant below T_C is revealed anomalously. We discuss the interpretation of these element-specific XMCD data based on the possible formation of an exotic ground state at low temperatures in the low-field limit.

II. EXPERIMENTAL CONDITIONS

A single crystal was synthesized using a previously described method [19,20]. Based on x-ray diffraction, the absence of undesired crystalline phases was confirmed. Energy-dispersive x-ray spectroscopy (Quanta 250 FEG, FEI) results show the actual composition of $\text{Fe}_{4.52}\text{Ge}_{1.02}\text{Te}_2$ ($x \approx 0.48$). For simplicity, we refer to our compound as Fe_5GeTe_2 hereinafter. Magnetometry measurements using an MPMS-3 (Quantum Design) revealed a T_C of approximately 310 K and absence of excessive iron atoms between the layers is judged (see Appendix A).

Soft x-ray absorption (XAS) measurements, including XMCD measurements, were performed at BL23SU of SPring-8, which was equipped with the twin-helical undulator that produce nearly perfectly left and right circularly polarized x rays [36]. For the cleaved single crystal in ultrahigh vacuum, all XAS spectra were captured by the total electron yield

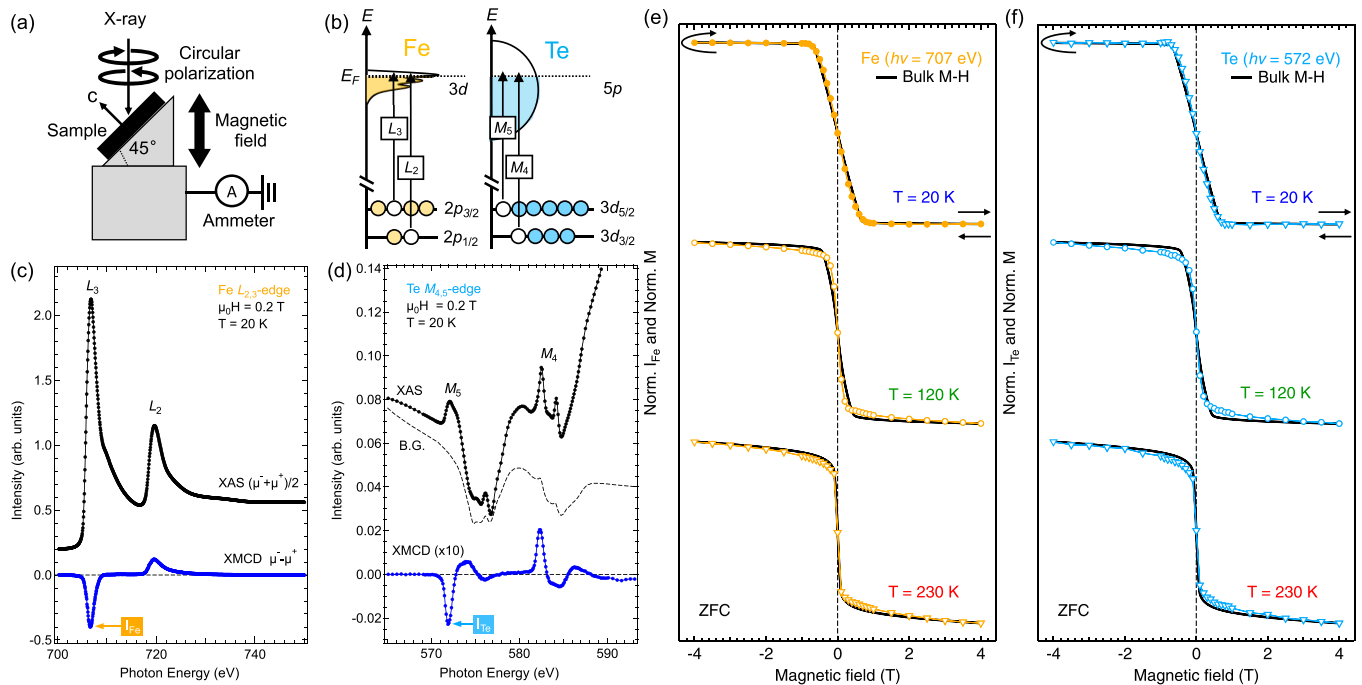


FIG. 2. (a) Geometry of XMCD measurements in total electron yield (TEY) mode with $\theta = 45^\circ$. XMCD spectra are defined as $\mu^- - \mu^+$, where μ^+ (μ^-) denotes absorption intensity for parallel (antiparallel) alignment of photon helicity and sample magnetization direction. (b) Schematic illustration of excitation process for Fe $L_{2,3}$ and Te $M_{4,5}$ edges. (c) Te $L_{2,3}$ -edge and (d) Te $M_{4,5}$ -edge XMCD spectra under 0.2 T at 20 K. Definition of characteristic intensities I_{Fe} and I_{Te} at L_3 (~ 707 eV) and M_5 (~ 572 eV) are indicated by horizontal arrows (see main text for details). In the Te $M_{4,5}$ edge, the background spectrum including the Cr $L_{2,3}$ edge (≈ 576 and 585 eV) absorption from the focusing mirrors in the BL23SU optical system is shown as the black solid line [34]. (e), (f) Comparison of magnetization curve shape between bulk M - H curves (with angle of induced magnetic field to sample surface normal direction θ of 45°), I_{Fe} - H curves, and I_{Te} - H curves. All data presented were obtained under zero-field cooling (ZFC) conditions and measured by changing the magnetic field, as indicated by the arrows. Within the resolution in our XMCD measurements, no hysteresis component was observed. In (e), (f), the signs of the M - H curves are reversed (see main text for details).

mode below the energy resolution of ~ 150 meV and then normalized by the incident photon flux. The XMCD spectra were obtained from $\mu^- - \mu^+$, where μ^+ (μ^-) denotes the XAS intensity corresponding to the parallel (antiparallel) orientations of the sample magnetization and incident photon helicity [Fig. 2(a)]. During data acquisition, the circular polarization at each photon energy was switched at a frequency of 1 Hz using five kicker magnets, which efficiently acquired XMCD data with a high signal to noise ratio. To eliminate experimental errors, the XAS/XMCD spectra with positive and negative magnetic fields were measured and averaged for each photon energy. We measured the XMCD signal based on a $\theta = 45^\circ$ geometry [see Fig. 2(a)] because the magnetic anisotropy energy was relatively low in this system [19,20]. To investigate the spin-polarized density of states for Fe $3d$ and Te $5p$ [see Fig. 2(b)], as in our previous study [34], we focused on the Fe $L_{2,3}$ and Te $M_{4,5}$ edges. The XMCD signal from Ge [34] is not discussed herein because of its low intensity.

III. RESULTS AND DISCUSSIONS

The XAS and XMCD spectra were measured under 0.2 and 4 T at 20, 120, and 230 K. Figures 2(c) and 2(d) show the XAS and XMCD spectra at 0.2 T and 20 K for the Fe $L_{2,3}$ and Te $M_{4,5}$ edges, respectively. Other XAS and XMCD spectra are provided in Appendix B. Consistent with previous

measurements, the Fe $L_{2,3}$ and Te $M_{4,5}$ edges appeared in the energy ranges of 690–760 and 565–595 eV, respectively. As discussed in our previous paper [34], disentangling the signal from nonequivalent Fe atomic sites is extremely difficult. Therefore, the XMCD signal for Fe is regarded as the summation of the signals from all nonequivalent Fe sites [see Fig. 1(a)]. For convenience, we define the XMCD intensity at the Fe L_3 (~ 707 eV) and Te M_5 (~ 572 eV) edges as I_{Fe} and I_{Te} , respectively [see colored horizontal arrows in Figs. 2(c) and 2(d)].

To confirm that the XMCD signal is intrinsic based on the bulk, bulk magnetization (M - H), I_{Te} - H , and I_{Fe} - H curves were compared. It is known that the sign of the XMCD signal is determined by the change in the orbital angular momentum Δl ($= I_{\text{final}} - I_{\text{initial}}$) during the excitation process. Because the sign of the XMCD at the $L_{2,3}$ and $M_{4,5}$ edges corresponding to the $p \rightarrow d$ ($\Delta l = 1$) and $d \rightarrow p$ processes ($\Delta l = -1$) [see Figs. 2(c) and 2(d)] is negative, we reversed the sign of the M - H curve to compare it with I_{Fe} and I_{Te} . Comparisons of I_{Fe} and I_{Te} between $+4$ T and -4 T are shown in Figs. 2(e) and 2(f), respectively. Within our measurement resolution, all bulk magnetometry and XMCD curves increased linearly and saturated within ± 1 T without indicating clear hysteresis. This behavior is similar to that observed for different sample configurations relative to the magnetic field, which suggests a slight magnetic anisotropy [34]. As shown in Figs. 2(e)

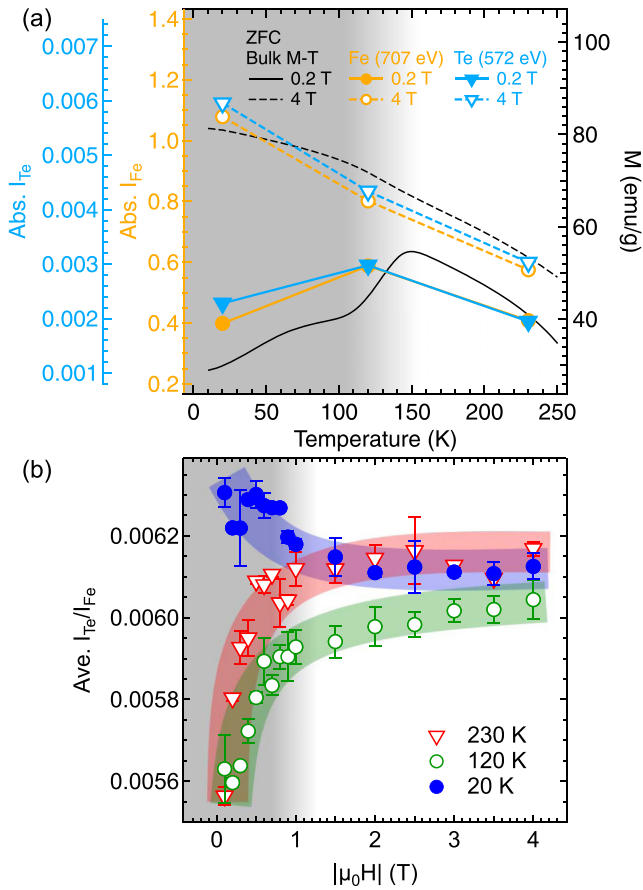


FIG. 3. (a) Temperature dependence of I_{Fe} and I_{Te} at 0.2 and 4 T. Here, I_{Fe} and I_{Te} are defined as the XMCD intensity at Fe L_3 (~ 707 eV) and Te M_5 (~ 572 eV), respectively [see Figs. 2(c) and 2(d)]. M - T curves (ZFC) from macroscopic magnetometry with $\theta = 45^\circ$ are shown as solid and dashed black lines. (b) Magnetic field dependence of averaged ratio $I_{\text{Te}}/I_{\text{Fe}}$ at 20, 120, and 230 K, as obtained from curves shown in Figs. 2(e) and 2(f). As no hysteresis component was observed, the averaged ratio $I_{\text{Te}}/I_{\text{Fe}}$ for positive and negative fields was plotted as a function of the absolute value of the external magnetic field ($|\mu_0 H|$). Error bar denotes variation in ratio between positive and negative fields. Data at $\mu_0 H = 0$ T were removed to avoid a mathematical singular point.

and 2(f), qualitatively similar M - H , I_{Fe} - H , and I_{Te} - H curve shapes were indicated for all temperatures. This intimate connection between XMCD and bulk magnetism was further confirmed by comparing the temperature evolutions of I_{Fe} and I_{Te} [Fig. 3(a)]. As temperature decreased, both I_{Fe} and I_{Te} at 4 T showed a systematic increase. By contrast with both I_{Fe} and I_{Te} at 4 T, the opposite behavior at 20 K was observed at 0.2 T. This characteristic difference in the magnetic signal between 0.2 and 4 T in the XMCD measurement is consistent with the bulk magnetometry data [solid and dashed black curves in Fig. 3(a)]. This confirms that our elemental-selective XMCD results reflect the intrinsic nature of the bulk electronic and the magnetic properties. A key advantage of element-specific XMCD, however, is its ability to extract unique information from bulk magnetometry.

To understand the element-specific nature of XMCD, we employed the relevant XMCD signal, $I_{\text{Te}}/I_{\text{Fe}}$. As shown in

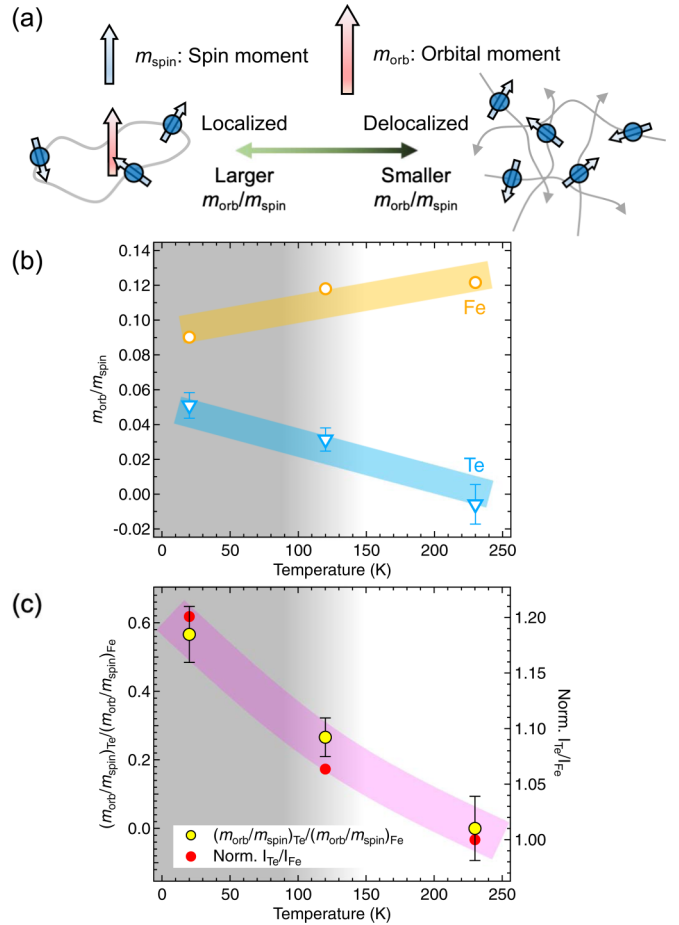


FIG. 4. (a) Schematic illustration of momentum from orbital (m_{orb}) and spin (m_{spin}) components (see main text for details). (b) Comparison of temperature-dependent $m_{\text{orb}}/m_{\text{spin}}$ between Fe and Te at 0.2 T. Opposite temperature dependences for Fe and Te are highlighted by lines. (c) Comparison between $(m_{\text{orb}}/m_{\text{spin}})_{\text{Te}}/(m_{\text{orb}}/m_{\text{spin}})_{\text{Fe}}$ and $I_{\text{Te}}/I_{\text{Fe}}$ at 0.2 T. Intimate scaling was observed between these two values (see main text for details). Details regarding estimation of error bar in panels (b,c) are provided in Appendix B.

Fig. 3(a), I_{Te} improved as compared with I_{Fe} at 20 K and 0.2 T. The enhancement in I_{Te} was further supported by a comparison of the magnetic field evolution of the $I_{\text{Te}}/I_{\text{Fe}}$ ratio among three temperatures of 20, 120, and 230 K [Fig. 3(b)]. Because no hysteresis component was present, we show the ratio only for the absolute field range after averaging the ratios for the positive and negative fields. In contrast to the 120 and 230 K cases, $I_{\text{Te}}/I_{\text{Fe}}$ was enhanced significantly in the low H-field region (< 1 T) at 20 K. The increased $I_{\text{Te}}/I_{\text{Fe}}$ ratio is particularly interesting because a stronger spin polarization of the Te 5p state is suggested by the enhancement in hybridization with the Fe 3d state. As will be shown later, this is supported by magneto-optical sum-rule analysis [37–39].

Magneto-optical sum-rule analysis can evaluate the relative magnetic moment ($m_{\text{orb}}/m_{\text{spin}}$) from the orbital (m_{orb}) and effective spin (m_{spin}) components of the target atom. As schematically shown in Fig. 4(a), intensifying the localized nature of the magnetic moment should result in a higher $m_{\text{orb}}/m_{\text{spin}}$ value, and intensifying the delocalized

nature should result in a lower $m_{\text{orb}}/m_{\text{spin}}$ value. Therefore, $m_{\text{orb}}/m_{\text{spin}}$ can indicate the hybridization degree qualitatively, as demonstrated in doping-induced ferromagnetic systems [40] and HF systems [41]. In the case of Fe_5GeTe_2 , because the Fe $3d$ and Te $5p$ electronic orbitals are localized and delocalized, respectively [see Fig. 1(c)], the temperature dependence of $m_{\text{orb}}/m_{\text{spin}}$ between Fe $3d$ and Te $5p$ is expected to exhibit opposite behaviors if the d - p hybridization is prominent. In this study, by focusing on XMCD in 0.2 T, we performed a magneto-optical sum-rule analysis for both the Fe $L_{2,3}$ and Te $M_{4,5}$ edges to estimate $m_{\text{orb}}/m_{\text{spin}}$. In fact, the $m_{\text{orb}}/m_{\text{spin}}$ for Fe can be calculated from the integration of the XMCD intensity for the overall L_3 edge (700–717 eV) and the overall $L_2 + L_3$ edge (700–750 eV) [Fig. 2(b)]. Similarly, the $m_{\text{orb}}/m_{\text{spin}}$ for Te can be calculated from the integration of the XMCD intensity for the overall M_5 edge (565–581 eV) and $M_4 + M_5$ edges (565–593 eV) [Fig. 2(c)]. Further details are available in Appendix B.

Figure 4(b) shows the temperature dependence of $m_{\text{orb}}/m_{\text{spin}}$ for the Fe $3d$ and Te $5p$ states at 0.2 T. By performing cooling, the $m_{\text{orb}}/m_{\text{spin}}$ value of Fe decreased, whereas that of Te increased. This contrasting trend can be reasonably attributed to a countereffect due to the increasing hybridization between delocalized Te $5p$ and localized Fe $3d$ orbitals [see Fig. 1(c)]. To further illustrate this contrasting trend, the ratio $(m_{\text{orb}}/m_{\text{spin}})_{\text{Te}}/(m_{\text{orb}}/m_{\text{spin}})_{\text{Fe}}$ was compared with $I_{\text{Te}}/I_{\text{Fe}}$ at 0.2 T [Fig. 4(c)]. The value of $(m_{\text{orb}}/m_{\text{spin}})_{\text{Te}}/(m_{\text{orb}}/m_{\text{spin}})_{\text{Fe}}$ reflects the enhancement degree of the localized nature of Te $5p$, and its excellent scaling with $I_{\text{Te}}/I_{\text{Fe}}$ led us to conclude that Fe $3d$ -Te $5p$ hybridization increases prominently with decreasing temperature in the low magnetic field limit.

At the phenomenological level, we discuss the connection between enhanced d - p hybridization and the anomalous ground state formation significantly below T_C . One possible scenario is the existence of CDW below ~ 150 K, as reported in recent publications [25,30]. The emergence of a CDW can cause band folding in the reciprocal lattice space owing to symmetry breaking by periodic lattice modulation, which is analogous to cases involving excitonic charge density wave materials TiSe_2 and ZrTe_2 [42,43]. For ferromagnetic metal Fe_5GeTe_2 , because the relatively localized Fe $3d$ band and delocalized Te $5p$ band are hybridized [34], band folding due to CDW results in more crossings between the Fe $3d$ and Te $5p$ bands, resulting in enhanced d - p hybridization. Supporting the low-dimensional double exchange model [44], the enhanced d - p hybridization can induce a relatively delocalized nature in the Fe $3d$ electrons [Figs. 4(a) and 4(b)] and the small but finite gap in the spin-polarized conduction band, which consequently weakens the ferromagnetism. Another possible scenario is the existence of an HF state, as proposed for Fe_3GeTe_2 [22,31]. The magnetic moment from Fe $3d$ electrons is screened by the spins of delocalized Te $5p$ electrons owing to the antiferromagnetic spin arrangement between localized Fe $3d$ and delocalized Te $5p$ electrons [34]. A d - p hybridized HF band is formed near E_F at low temperatures, consequently resulting in the suppression of ferromagnetism, as in HF systems [7,8]. Our temperature-dependent XMCD results [see Appendix B] do not contradict both the CDW and HF scenarios below 150 K. If these CDW and/or HF formation

scenarios are in fact correct, then the melting of the CDW and/or Kondo lattice by applying an external field above ~ 1 T is expected, based on the magnetic field evolution of $I_{\text{Te}}/I_{\text{Fe}}$ at 20 K [see blue curve in Fig. 3(b)].

IV. SUMMARY

In summary, we demonstrated the temperature and magnetic field dependence of element-specific XMCD measurements in a Fe_5GeTe_2 system. Based on a cooled sample, a systematic increase in the magnetic moment of the Te $5p$ state due to enhanced $3d$ - $5p$ hybridization was clarified. Whereas the ligand state has been regarded as a less significant component compared with the Fe $3d$ orbitals, the enhancement of its hybridization with the $5p$ orbital in heavy element Te should not be underestimated for modeling the ground state magnetic background, and hence its excited states. In particular, the significant spin-orbital coupling effect from heavy element Te might modify the magnetic crystalline and exchange anisotropies. Because an intrinsic large tunability of occupation exists at the Fe(1) site, which is the nearest Fe site to the Te atomic sheet, our findings provide important information for identifying exotic magnetic ground states and their excited states in Fe_5GeTe_2 . We believe that the findings presented herein would facilitate the deeper understanding of itinerant magnetism in low-dimensional systems, as many itinerant magnetic chalcogenides contain heavy Te. Furthermore, in this study, XMCD measurements were clearly demonstrated as one of the most effective methods for clarifying near- E_F element-specific spin-polarized electronic states, particularly for materials with intrinsically complicated band structures.

ACKNOWLEDGMENTS

The crystal structure shown in Fig. 1(a) was depicted using VESTA [51]. This work was supported by JSPS KAKENHI (Grant No. 19K15580). This work was performed under the Shared Use Program of JAEA Facilities (Proposal No. 2020A-E20) with the approval of Nanotechnology Platform project supported by the Ministry of Education, Culture, Sports, Science and Technology (Proposal No. JPMXP09A20AE0020). The synchrotron radiation experiments were performed at JAEA beamline BL23SU in Spring-8 (Proposal No. 2020A3844).

APPENDIX A: MAGNETIC CHARACTERIZATION

The atomic layer of our quenched Fe_5GeTe_2 single crystal has been already obtained by the cross-section TEM images, indicating the absence of the iron atoms between layers [29]. In this study, we indirectly examined the confirmation of the absence of the intercalated iron atoms and the magnetic characterization by measuring the macroscopic magnetometry using an MPMS-3 (Quantum Design). Figures 5(a) and 5(b) show the M - T curves measured for in-plane ($H//ab$) and out of plane ($H//c$) field with 10 mT under the zero-field cooling process. Our single-crystal sample has a T_C of approximately 310 K [Fig. 5(b)], which is larger than that of Fe_4GeTe_2 ($T_C \sim 280$ K) [21]. Additionally, in $H//ab$ geometry, three bumps were observed at ~ 275 , ~ 180 , and ~ 110 K. Since the mean-field theory shows that the spontaneous magnetization

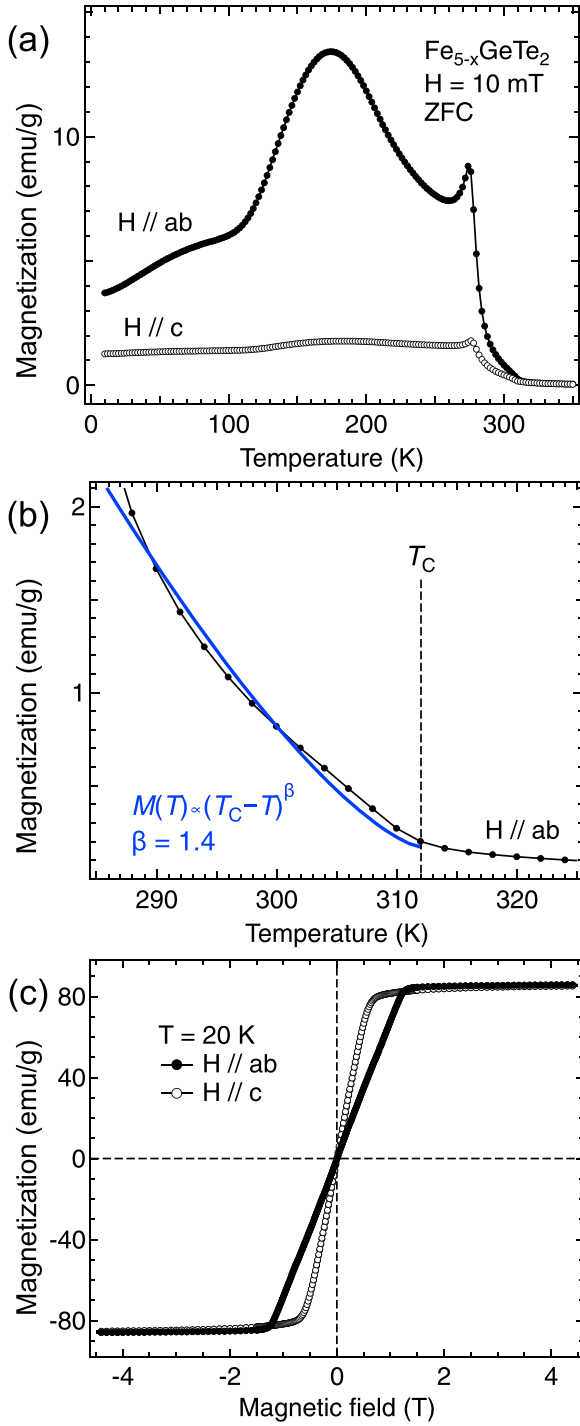


FIG. 5. (a) M - T curve measured for in-plane (black solid line with full circle, $H//ab$) and out of plane (black solid line with circle, $H//c$) field with 10 mT under the zero-field cooling process. (b) M - T curve in $H//ab$ near T_C . The fitting results of a power-law dependence of the spontaneous magnetization (M_S) on the reduced temperature $M_S(T) \propto (T_C - T)^\beta$ with $\beta = 1.4$, based on the mean-field model, is also shown. (c) M - H curve measured for $H//ab$ and $H//c$ at 20 K.

(M_S) has a power-law dependence on the reduced temperature, we applied a power-law $M_S(T) \propto (T_C - T)^\beta$ fitting to the M - T curve near T_C [45]. The best reproduced fitting is when $\beta = 1.4$, which is larger than Fe_3GeTe_2 (0.37) [46]

and the mean-field model value (0.5) [47]. Figure 5(c) shows the M - H curve measured for in-plane ($H//ab$) and out of plane ($H//c$) field at 20 K; its magnetic anisotropy is smaller than that of Fe_nGeTe_2 ($n = 3, 4$) [14,29,48]. These unique temperature and field features are consistent with those in the previous literature for Fe_5GeTe_2 without iron atoms between the layers [19,23]. Therefore, we judged that our measured single-crystal sample has few intercalated iron atoms.

APPENDIX B: MAGNETO-OPTICAL SUM-RULE ANALYSIS

This Appendix shows the details of the estimation of $m_{\text{orb}}/m_{\text{spin}}$ using the magneto-optical sum-rule analysis, being associated with Fig. 4(b) in the main text. Figure 6 shows the temperature dependence of the integral XMCD spectra ($\int \mu^- - \mu^+$) under $\mu_0 H = 0.2$ T at Fe $L_{2,3}$ and Te $M_{4,5}$ edges together with their XAS and XMCD spectra. According to the magneto-optical sum rule, for arbitrary elements with a spin-polarized state, the expectation value of orbital ($m_{\text{orb}} = -\langle L_z \rangle$) and spin ($m_{\text{spin}} = -2\langle S_{z,\text{eff}} \rangle$) contributions to the total magnetic moment ($m_{\text{total}} = m_{\text{orb}} + m_{\text{spin}}$) is calculated by using the following equations [37,38]:

$$m_{\text{orb}} = -\frac{2l(l+1)}{l(l+1) + 2 - c(c+1)} (4l + 2 - n) \frac{q}{\frac{3}{2}r}, \quad (\text{B1})$$

$$m_{\text{spin}} = -\frac{6c}{l(l+1) - 2 - c(c+1)} (4l + 2 - n) \times \frac{\frac{2c+1}{c}p - \frac{c+1}{c}q}{\frac{3}{2}r}, \quad (\text{B2})$$

where l and c denote the orbital angular momentum at valence and core level in the $c \rightarrow l$ dipole transition. Fe $L_{2,3}$ ($p \rightarrow d$) and Te $M_{4,5}$ ($d \rightarrow p$) edges correspond to the $(c, l) = (1, 2), (2, 1)$, respectively. The major role parameters in Eqs. (B1) and (B2) are p , q , and r . p and q correspond to the integral XMCD signal over the j_+ edge and $j_+ + j_-$ edge, where $j_\pm = c \pm 1/2$ is a spin-orbit split core-level edge. r denotes the integral XAS signal over the $j_+ + j_-$ edge, where the XAS signal to be integrated has removed the background. m_{spin} contains two expectation values of the spin-magnetic moment $\langle S_z \rangle$ and the magnetic dipole operator $\langle T_z \rangle$. In the metallic iron, the $\langle T_z \rangle$ contribution is a few or less percent of $\langle S_z \rangle$ [39]. Since Fe $L_{2,3}$ -edge XAS spectra of Fe_5GeTe_2 behaves as the metallic state, the $\langle T_z \rangle$ contribution can be negligible in this study. In addition to the $\langle T_z \rangle$ value, the number of electrons (n) in Eqs. (B1) and (B2) can be estimated using theoretical band calculations. However, the complex band structure due to the high structural degrees of freedom of the occupied Fe sites gives rise to numerical uncertainties, which lead to increase m_{orb} and m_{spin} uncertainties. Therefore, it is advantageous to cancel out n using the relative magnetic moment $m_{\text{orb}}/m_{\text{spin}}$ by using the following equation:

$$\frac{m_{\text{orb}}}{m_{\text{spin}}} = \frac{2l(l+1)\{l(l+1) - 2 - c(c+1)\}}{6c\{l(l+1) + 2 - c(c+1)\}} \frac{1}{\frac{2c+1}{c}(\frac{p}{q}) - \frac{c+1}{c}}. \quad (\text{B3})$$

Even if there is a complex background in the XAS spectra, such as at the Te $M_{4,5}$ edge [see Fig. 2(d) or Fig. 6], the specific

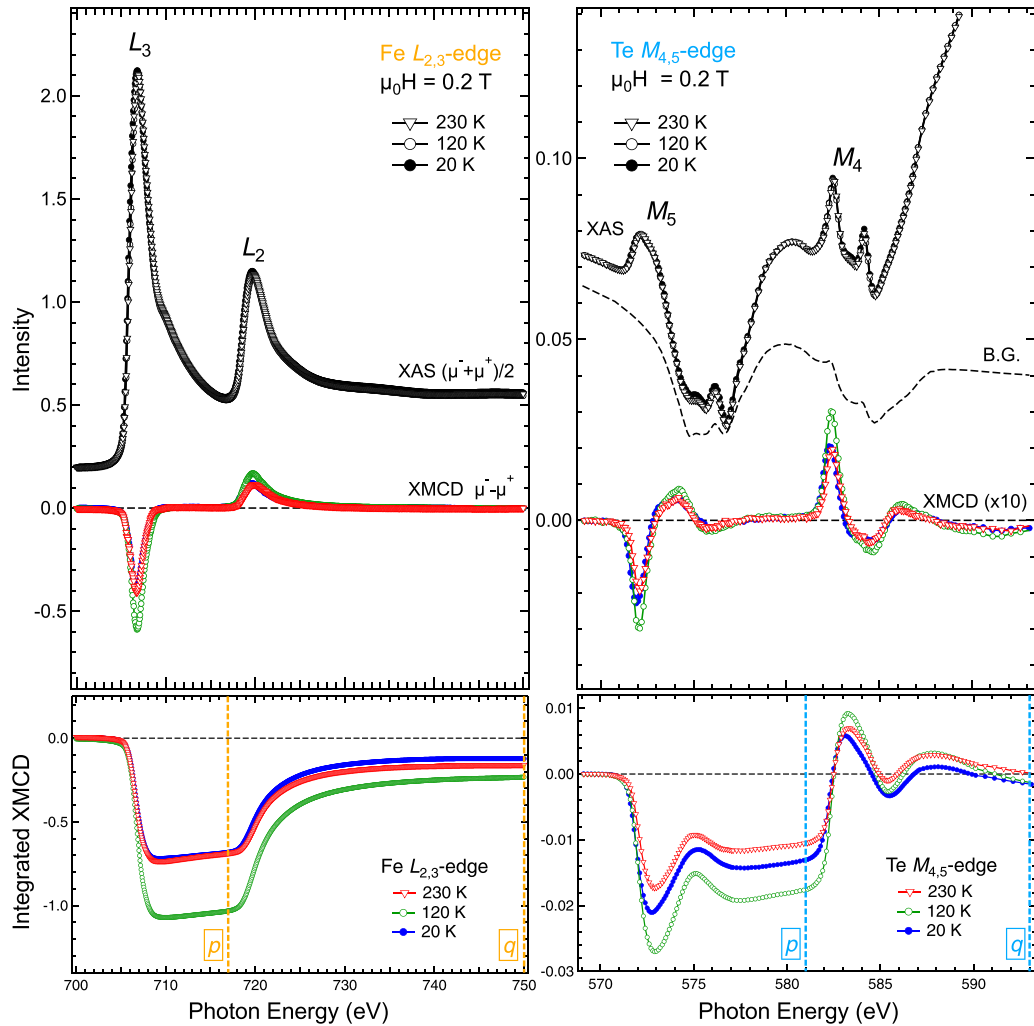


FIG. 6. Fe $L_{2,3}$ - and Te $M_{4,5}$ -edge integral XMCD spectra of Fe_5GeTe_2 at three temperatures (20, 120, and 230 K) under $\mu_0 H = 0.2$ T. The XAS and XMCD spectra, presented in Figs. 2(c) and 2(d) in the main text, are shown at the same time. In integral XMCD spectra, the p and q is shown as the vertical dashed line with color.

form has the advantage of directly linking the integral XMCD ratio to the relative magnetic moment. The increasing of the p/q value reflects the smaller $m_{\text{orb}}/m_{\text{spin}}$ value, indicating the relative delocalization [see Fig. 4(a) in the main text]. By using Eq. (B3), the degree of the localization/delocalization has been discussed, such as the doping-induced ferromagnetic system [40] and heavy fermion system [41]. In this study, we apply Eq. (B3) to both the Fe $L_{2,3}$ and Te $M_{4,5}$ edges.

Since the XMCD signal is about ten times smaller than the XAS signal, the uncertainty of the p and q values may affect the $m_{\text{orb}}/m_{\text{spin}}$ results. Therefore, we carefully considered the photon energy ($h\nu$) corresponding to the p and q values. In the Fe $L_{2,3}$ edge, the q value can be precisely determined since there are no other XAS and XMCD spectra observed within

the Fe $L_{2,3}$ edge. The p value can be determined by choosing a cutoff at the onset of the L_2 edge. Note that a slight uncertainty in the p value will not significantly change the $m_{\text{orb}}/m_{\text{spin}}$ value, because p is much larger than q in Fe $L_{2,3}$ [39]. We set the p and q values for the Fe $L_{2,3}$ edge at $h\nu = 717$ and 750 eV (vertical orange dashed lines). In contrast, in the Te $M_{4,5}$ edge, the large s - d - f hybrid main edge [49] above 590 eV is close to the Te $M_{4,5}$ edge [see Fig. 2(d) or Fig. 6]. However, since the XMCD from the s - d - f main edge has been small [50], we think that the uncertainty in the q value is small enough. We set the p and q values for the Te $M_{4,5}$ edge at $h\nu = 581$ and 593 eV (vertical light blue dashed lines). The error bars at each absorption edge were evaluated by varying the photon energy of the q value in the range of ± 0.5 eV.

- [1] M. Imada, A. Fujimori, and Y. Tokura, *Rev. Mod. Phys.* **70**, 1039 (1998).
 [2] Y. Tokura and N. Nagaosa, *Science* **288**, 462 (2000).
 [3] E. Dagotto, *Science* **309**, 257 (2005).

- [4] C. M. Varma, *Rev. Mod. Phys.* **48**, 219 (1976).
 [5] J. M. Lawrence, P. S. Riseborough, and R. D. Parks, *Rep. Prog. Phys.* **44**, 1 (1981).
 [6] G. R. Stewart, *Rev. Mod. Phys.* **56**, 755 (1984).

- [7] S. Doniach, *Physica B+C* **91**, 231 (1977).
- [8] Z. F. Weng, M. Smidman, L. Jiao, X. Lu, and H. Q. Yuan, *Rep. Prog. Phys.* **79**, 094503 (2016).
- [9] F. C. Zhang and T. M. Rice, *Phys. Rev. B* **37**, 3759 (1988).
- [10] B. Keimer, S. A. Kivelson, M. R. Norman, S. Uchida, and J. Zaanen, *Nature (London)* **518**, 179 (2015).
- [11] A. K. Geim and I. V. Grigorieva, *Nature (London)* **499**, 419 (2013).
- [12] C. Gong and X. Zhang, *Science* **363**, 706 (2019).
- [13] S. Yang, T. Zhang, and C. Jiang, *Adv. Sci.* **8**, 2002488 (2021).
- [14] B. Chen, J. H. Yang, H. D. Wang, M. Imai, H. Ohta, C. Michioka, K. Yoshimura, and M. H. Fang, *J. Phys. Soc. Jpn.* **82**, 124711 (2013).
- [15] Z. Fei, B. Huang, P. Malinowski, W. Wang, T. Song, J. Sanchez, W. Yao, D. Xiao, X. Zhu, A. F. May, W. Wu, D. H. Cobden, J.-H. Chu, and X. Xu, *Nat. Mater.* **17**, 778 (2018).
- [16] G. D. Nguyen, J. Lee, T. Berlijn, Q. Zou, S. M. Hus, J. Park, Z. Gai, C. Lee, and A.-P. Li, *Phys. Rev. B* **97**, 014425 (2018).
- [17] Y. Deng, Y. Yu, Y. Song, J. Zhang, N. Z. Wang, Z. Sun, Y. Yi, Y. Z. Wu, S. Wu, J. Zhu, J. Wang, X. H. Chen, and Y. Zhang, *Nature (London)* **563**, 94 (2018).
- [18] Y.-P. Wang, X.-Y. Chen, and M.-Q. Long, *Appl. Phys. Lett.* **116**, 092404 (2020).
- [19] A. F. May, D. Ovchinnikov, Q. Zheng, R. Hermann, S. Calder, B. Huang, Z. Fei, Y. Liu, X. Xu, and M. A. McGuire, *ACS Nano* **13**, 4436 (2019).
- [20] A. F. May, C. A. Bridges, and M. A. McGuire, *Phys. Rev. Materials* **3**, 104401 (2019).
- [21] J. Seo, D. Y. Kim, E. S. An, K. Kim, G.-Y. Kim, S.-Y. Hwang, D. W. Kim, B. G. Jang, H. Kim, G. Eom, S. Y. Seo, R. Stanina, M. Muntwiler, J. Lee, K. Watanabe, T. Taniguchi, Y. J. Jo, J. Lee, B. Il Min, M. H. Jo *et al.*, *Sci. Adv.* **6**, eaay8912 (2020).
- [22] Y. Zhang, H. Lu, X. Zhu, S. Tan, W. Feng, Q. Liu, W. Zhang, Q. Chen, Y. Liu, X. Luo, D. Xie, L. Luo, Z. Zhang, and X. Lai, *Sci. Adv.* **4**, eaao6791 (2018).
- [23] H. Zhang, R. Chen, K. Zhai, X. Chen, L. Caretta, X. Huang, R. V. Chopdekar, J. Cao, J. Sun, J. Yao, R. Birgeneau, and R. Ramesh, *Phys. Rev. B* **102**, 064417 (2020).
- [24] J. Seo, E. S. An, T. Park, S.-Y. Hwang, G.-Y. Kim, K. Song, W.-S. Noh, J. Y. Kim, G. S. Choi, M. Choi, E. Oh, K. Watanabe, T. Taniguchi, J. -H. Park, Y. J. Jo, H. W. Yeom, S.-Y. Choi, J. H. Shim, and J. S. Kim, *Nat. Commun.* **12**, 2844 (2021).
- [25] Y. Gao, Q. Yin, Q. Wang, Z. Li, J. Cai, T. Zhao, H. Lei, S. Wang, Y. Zhang, and B. Shen, *Adv. Mater.* **32**, 2005228 (2020).
- [26] B. Ding, Z. Li, G. Xu, H. Li, Z. Hou, E. Liu, X. Xi, F. Xu, Y. Yao, and W. Wang, *Nano Lett.* **20**, 868 (2020).
- [27] T. J. Kim, S. Ryee, and M. J. Han, [arXiv:2202.02022](https://arxiv.org/abs/2202.02022).
- [28] K. Kim, J. Seo, E. Lee, K.-T. Ko, B. S. Kim, B. G. Jang, J. M. Ok, J. Lee, Y. J. Jo, W. Kang, J. H. Shim, C. Kim, H. W. Yeom, B. I. Min, B.-J. Yang, and J. S. Kim, *Nat. Mater.* **17**, 794 (2018).
- [29] T. Ohta, K. Sakai, H. Taniguchi, B. Driesen, Y. Okada, K. Kobayashi, and N. Niimi, *Appl. Phys. Express* **13**, 043005 (2020).
- [30] X. Wu, L. Lei, Q. Yin, N.-N. Zhao, M. Li, Z. Wang, Q. Liu, W. Song, H. Ma, P. Ding, Z. Cheng, K. Liu, H. Lei, and S. Wang, *Phys. Rev. B* **104**, 165101 (2021).
- [31] M. Zhao, B.-B. Chen, Y. Xi, Y. Zhao, H. Xu, H. Zhang, N. Cheng, H. Feng, J. Zhuang, F. Pan, X. Xu, W. Hao, W. Li, S. Zhou, S. X. Dou, and Y. Du, *Nano Lett.* **21**, 6117 (2021).
- [32] M. Joca, U. Yang, and C. Lee, *Nano Mater. Sci.* **1**, 299 (2019).
- [33] T. T. Ly, J. Park, K. Kim, H.-B. Ahn, N. J. Lee, K. Kim, T.-E. Park, G. Duvjir, N. H. Lam, K. Jang, C.-Y. You, Y. Jo, S. K. Kim, C. Lee, S. Kim, and J. Kim, *Adv. Funct. Mater.* **31**, 2009758 (2021).
- [34] K. Yamagami, Y. Fujisawa, B. Driesen, C. H. Hsu, K. Kawaguchi, H. Tanaka, T. Kondo, Y. Zhang, H. Wadati, K. Araki, T. Takeda, Y. Takeda, T. Muro, F. C. Chuang, Y. Niimi, K. Kuroda, M. Kobayashi, and Y. Okada, *Phys. Rev. B* **103**, L060403 (2021).
- [35] X. Yang, X. Zhou, W. Feng, and Y. Yao, *Phys. Rev. B* **104**, 104427 (2021).
- [36] Y. Saitoh, Y. Fukuda, Y. Takeda, H. Yamagami, S. Takahashi, Y. Asano, T. Hara, K. Shirasawa, M. Takeuchi, T. Tanaka, and H. Kitamura, *J. Synchrotron Radiat.* **19**, 388 (2012).
- [37] B. T. Thole, P. Carra, F. Sette, and G. van der Laan, *Phys. Rev. Lett.* **68**, 1943 (1992).
- [38] P. Carra, B. T. Thole, M. Altarelli, and X. Wang, *Phys. Rev. Lett.* **70**, 694 (1993).
- [39] C. T. Chen, Y. U. Idzerda, H.-J. Lin, N. V. Smith, G. Meigs, E. Chaban, G. H. Ho, E. Pellegrin, and F. Sette, *Phys. Rev. Lett.* **75**, 152 (1995).
- [40] L. R. Shelford, T. Hesjedal, L. Collins-McIntyre, S. S. Dhesi, F. Maccherozzi, and G. van der Laan, *Phys. Rev. B* **86**, 081304(R) (2012).
- [41] T. Okane, Y. Takeda, H. Yamagami, A. Fujimori, Y. Matsumoto, N. Kimura, T. Komatsubara, and H. Aoki, *Phys. Rev. B* **86**, 125138 (2012).
- [42] H. Cercellier, C. Monney, F. Clerc, C. Battaglia, L. Despont, M. G. Garnier, H. Beck, P. Aebi, L. Patthey, H. Berger, and L. Forró, *Phys. Rev. Lett.* **99**, 146403 (2007).
- [43] Y. Song, C. Jia, H. Xiong, B. Wang, Z. Jiang, K. Huang, J. Hwang, Z. Li, C. Hwang, Z. Liu, D. Shen, J. Sobota, P. Kirchmann, J. Xue, T. P. Devereaux, S.-K. Mo, Z.-X. Shen, and S. Tang, [arXiv:2201.11592](https://arxiv.org/abs/2201.11592).
- [44] S. Nishimoto and Y. Ohta, *Phys. Rev. Lett.* **109**, 076401 (2012).
- [45] M. E. Fisher, *Rep. Prog. Phys.* **30**, 615 (1967).
- [46] Y. Liu, V. N. Ivanovski, and C. Petrovic, *Phys. Rev. B* **96**, 144429 (2017).
- [47] J. M. Lu, O. Zheliuki, I. Leermakers, N. F. Q. Yuan, U. Zeitler, K. T. Lawand, and J. T. Ye, *Science* **350**, 1353 (2015).
- [48] Z. Li, W. Xia, H. Su, Z. Yu, Y. Fu, L. Chen, X. Wang, N. Yu, Z. Zou, and Y. Guo, *Sci. Rep.* **10**, 15345 (2020).
- [49] K. Takubo, R. Comin, D. Ootsuki, T. Mizokawa, H. Wadati, Y. Takahashi, G. Shibata, A. Fujimori, R. Sutarto, F. He, S. Pyon, K. Kudo, M. Nohara, G. Levy, I. S. Elfimov, G. A. Sawatzky, and A. Damascelli, *Phys. Rev. B* **90**, 081104(R) (2014).
- [50] M. Ye, T. Xu, G. Li, S. Qiao, Y. Takeda, Y. Saitoh, S.-Y. Zhu, M. Nurmamat, K. Sumida, Y. Ishida, S. Shin, and A. Kimura, *Phys. Rev. B* **99**, 144413 (2019).
- [51] K. Momma and F. Izumi, *J. Appl. Crystallogr.* **44**, 1272 (2011).